Journal of Organometallic Chemistry 881 (2019) 58–65

Contents lists available at ScienceDirect

Journal of Organometallic Chemistry

journal homepage: www.elsevier.com/locate/jorganchem

Synthesis and characterization of an acidic nanostructure based on magnetic polyvinyl alcohol as an efficient heterogeneous nanocatalyst for the synthesis of α-aminonitriles

Ali Maleki*, Jamal Rahimi, Zoleikha Hajizadeh, Maryam Niksefat

Catalysts and Organic Synthesis Research Laboratory, Department of Chemistry, Iran University of Science and Technology, Tehran, 16846-13114, Iran

A R T I C L E I N F O

Article history:
Received 29 October 2018
Received in revised form
27 November 2018
Accepted 3 December 2018
Available online 5 December 2018

Keywords:
Polyvinyl alcohol
Nanocomposite
Magnetic nanocatalyst
Sulfonic acid
α-Aminonitrile
Green chemistry

A B S T R A C T

The present study described design, preparation and characterization of a new magnetic nanocomposite based on polyvinyl alcohol (PVA) as a non-toxic, water-soluble, high mechanical stable and low-cost polymer. Fourier transform infrared (FT-IR) spectroscopy, field-emission scanning electron microscopy (FE-SEM) image, transmission electron microscope (TEM) image, X-ray diffraction (XRD) pattern, energy-dispersive X-ray (EDX) analysis and thermogravimetric (TG) analysis were used to describe the morphological, chemical and physical properties of the prepared nanocatalyst. All these results confirmed the successful synthesis of Fe_3O_4@PVA-SO_3H. This heterogeneous nanocatalyst was then successfully used for the synthesis of α-aminonitrile derivatives by starting from an aldehyde, an aniline and trimethylsilyl cyanide (TMSCN). High efficiency, green chemistry properties, simple and easy separation are the specific properties of this nanocomposite. Fe_3O_4@PVA-SO_3H can be derived out by an external magnet and reused ten times without any changes in its structure.

1. Introduction

By looking more closely at the needs of industry, developing new catalysts based on green chemistry principals is urgently needed. Nowadays, nanomaterials have been exhibited significant advantages and features due to their large surface-to-volume ratio [1–15]. The difficulty of separating nanocatalyst from reaction media extremely limits their applications in industry. To conquer this drawback in the last decade's magnetic nanoparticles (MNPs) gained considerable attention [16]. Among the magnetic nanoparticles, Fe_3O_4 nanoparticles have been recognized the most widely used due to its properties such as low cost, relative high magnetic saturation, and easy preparation [17]. To prevent agglomeration and oxidation of Fe_3O_4 NPs coating with organic and inorganic materials including small molecules, silica, polymers, carbon, metal or metal oxide NPs is urgently needed [18,19]. Also, the coating procedures provide reaction sites or active groups for covalently or no covalently grafting the active catalytic units onto the coated MNPs to construct magnetically recoverable catalysts.

PVA can be used as a high performance polymer because of the unique combination of beneficial properties such as non-toxicity, water-solubility, biocompatibility, biodegradability, low cost and high mechanical efficiency [20]. Its high hydrophilicity and high surface –OH groups lead to easy modification by different nanoparticles and can decrease the aggregation process [21]. The effective immobilization of the Fe_3O_4 inside the PVA was achieved by their bonding with the exposed hydroxyl groups in PVA.

There are several protocols reported in the literature for synthesizing Fe_3O_4/PVA nanocomposites such as *in situ* [22], ex-situ methods [23], and sonochemical method [24]. The reported methods have their own advantages and disadvantages but, the *in situ* method gives more homogenate composite in relatively short time. The application of this nanocomposite has been investigated in many different fields such as in drug delivery [25], as membranes for bone regeneration [26], as magneto-thermal for hyperthermia in cancer [25], an enzyme carrier [27] and biomedical application [28].

Recently, due to high reactivity, operational simplicity, low toxicity, non-corrosive nature and recoverable properties heterogeneous acid catalysts are found as an effective catalyst for the organic reactions [29,30]. The three-component synthesis of α-aminonitriles via Strecker reaction was carried out by the combination of aldehydes, amines and TMSCN. Aminonitriles are versatile

* Corresponding author.
E-mail address: maleki@iust.ac.ir (A. Maleki).

https://doi.org/10.1016/j.jorganchem.2018.12.002
0022-328X/

intermediates for the synthesis of amino acids via hydrolysis of the nitrile moiety [31]. Many methods have been developed for the synthesis of aminonitriles by use of acid catalysts such as $InCl_3$ [32], $BiCl_3$ [33] and $CoCl_2$ [34].

In continuation of last research on green nanocatalyst and organic synthesis [35,36], herein, the synthesis and characterization of Fe_3O_4@PVA-SO_3H nanocomposite were investigated for the first time and its application as a nanocatalyst was examined in the synthesis of aminonitriles via Strecker reaction (Scheme 1).

2. Experimental

2.1. General

All the solvents, reagents, and chemicals were purchased from Merck, Fluka and Aldrich. FT-IR spectra were recorded on a Shimadzu IR-470 spectrometer by the method of KBr pellets. Melting points were measured on an Electrothermal 9100 apparatus and are uncorrected. Field-emission scanning electron microscopy (FE-SEM) images were taken with KYKY-EM3200. Transmission electron microscope (TEM) image was obtained by Philips CM120. X-ray (EDX) analysis was recorded with a Numerix DXP–X10P. Thermal analysis was taken by Bahr-STA 504 instrument in the air atmosphere. XRD patterns of the solid powders were carried out using a JEOL JDX–8030 (30 kV, 20 mA). The products were identified by comparison of their spectroscopic and analytical data with those of authentic samples.

2.2. Preparation of Fe_3O_4@PVA nanocomposite

Fe_3O_4@PVA nanoparticles were synthesized by co-precipitation method. At first, 2.0 g of PVA 72000 Mw was dissolved in 40 mL water at 80 °C for 6 h to achieve homogenous mixture. The homogenous PVA was mixed with 12 mL of $NH_3.H_2O$ in a three-necked flask under nitrogen (N_2) atmosphere. Then, 2.5 g of $FeCl_3.6H_2O$ and 1.0 g of $FeCl_2.4H_2O$ were dissolved in 10 mL of deionized water. The mixture of $FeCl_3.6H_2O$ and $FeCl_2.4H_2O$ was added slowly to the NH_3– PVA solution and the mixture heated at 60 °C for 120 min. The obtained Fe_3O_4@PVA precipitate was washed with deionized water until pH was reached to 7. Finally, it was dried at 80 °C in an oven.

2.3. Preparation of Fe_3O_4@PVA-SO_3H nanoparticles

Functionalizing of prepared Fe_3O_4@PVA nanocomposite with SO_3H, was done by using a suction flask equipped with a constant-pressure dropping funnel and a gas inlet tube for conducting HCl gas over an absorbing solution (i.e., water), charged with the Fe_3O_4@PVA (0.5 g) in CH_2Cl_2 (20 mL) and dispersed by an ultrasonic bath for 30 min. Then, a solution of chlorosulfonic acid (0.25 mL) in CH_2Cl_2 (5 mL) was added dropwise at −10 °C during 30 min. After the addition was completed, the mixture was stirred for 90 min until HCl was fetched up completely. A powder of nano-Fe_3O_4@PVA-SO_3H was obtained. The nanocomposite was filtered and washed several times with dry CH_2Cl_2, methanol and distilled water. The precipitate was dried under vacuum at 70 °C.

2.4. General procedure for the synthesis of 2-(N-anilino)-2-phenyl acetonitrile **4a-z**

The Mixture of benzaldehyde (0.107 g, 1 mmol), aniline (0.093 g, 1 mmol) and TMSCN (0.120 g, 1.2 mmol) in 3 mL of EtOH was stirred for 10 min at ambient temperature in the presence of Fe_3O_4@PVA-SO_3H nanocomposite (0.050 g). The completion of the reaction was monitored by TLC (ethyl acetate–n-hexane, 1:3). Catalyst was separated easily by an external magnet. The pure crystalline products were achieved from the reaction mixture by recrystallization in hot EtOH.

3. Results and discussion

In this work, Fe_3O_4@PVA-SO_3H heterogeneous acidic nanocatalyst was synthesized for the first time under mild conditions and short reaction times. As can be seen in Scheme 1, Fe_3O_4@PVA-SO_3H nanocatalyst was prepared after two steps. At first, Fe_3O_4@PVA nanoparticles were synthesized by co-precipitation method in presence of PVA and solution of $FeCl_3.6H_2O$ and $FeCl_2.4H_2O$ under N_2. After that, Fe_3O_4@PVA was treated by chlorosulfonic acid to synthesize Fe_3O_4@PVA-SO_3H nanocatalyst. Various methods have been used to confirm synthesis the nanocomposite. FT-IR spectra for confirming the incorporation of SO_3H onto Fe_3O_4@PVA, Energy-dispersive X-ray (EDX) for the elemental analysis, The field emission scanning electron microscopy (FE-SEM) for morphology and the size details of synthesized nanocomposite, X-ray diffraction (XRD) for crystalline phases of Fe_3O_4@PVA-SO_3H

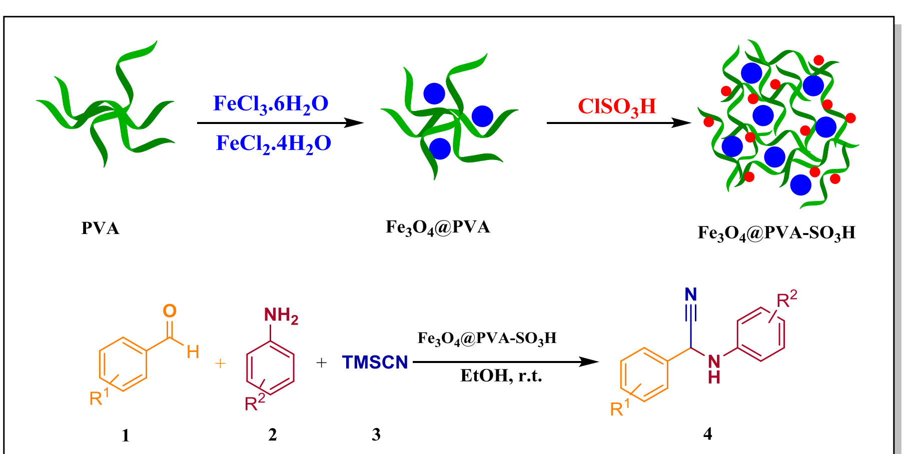

Scheme 1. Preparation of Fe_3O_4@PVA-SO_3H and catalytic application in the α-aminonitrile derivatives.

and The thermogravimetric analysis (TGA) for thermal stability, which are discussed as follow.

3.1. Characterization of the nanocomposite

3.1.1. FT-IR analysis

FT-IR spectroscopy, Fig. 1, confirmed the formation of the nanocomposite. The bending vibration band of Fe—O appeared at 584 cm^{-1}. The O—H stretch of Fe_3O_4 and PVA appeared around 3400, and confirm the presence of a great number of PVA hydroxyl functional groups that can be easy modified by SO_3H groups. Stretching vibration band at 2923 is regarding to C—H of PVA [37]. The S—O stretching vibrations of SO_3H groups in Fe_3O_4-PVA-SO_3H nanocomposite on Fe_3O_4@PVA surface appeared at 1124 cm^{-1} that indicated the synthesis of Fe_3O_4@PVA-SO_3H [38]. Finally, as can be seen, we have characterized the recycled nanocatalyst by FT-IR spectroscopy which showed suitable retention of its structure and there was no considerable deformation or leaching after ten times reusing.

3.1.2. Energy-dispersive X-ray (EDX)

The EDX elemental analysis of the Fe_3O_4@PVA-SO_3H MNPs was shown in Fig. 2. This analysis strongly clarifies that the SO_3H groups were successfully incorporated onto the magnetic PVA. It approved the presence of carbon, oxygen and sulfur elements in the nanocomposite and confirmed the purity of the nanocomposite.

3.1.3. Field-emission scanning electron microscopy (FE-SEM)

The FE-SEM images of the outer surface of the Fe_3O_4@PVA-SO_3H nanocomposite is illustrated in Fig. 3. A close examination of the figure revealed that the iron oxide impregnated in the polymer matrix and embedded in a sponge-like PVA matrix also, The Fe_3O_4 nanoparticles exhibit cubic structure. Furthermore, iron oxide particles show the uniform size of nanometer dimensions with the range of average diameter 40.27 ± 6 nm.

3.2. Transmission electron microscope (TEM)

TEM image micrograph of Fe_3O_4@PVA-SO_3H nanocomposite was illustrated in Fig. 4. It clearly shows considerable exfoliation of PVA after functionalized by Fe_3O_4 and SO_3H by nearly

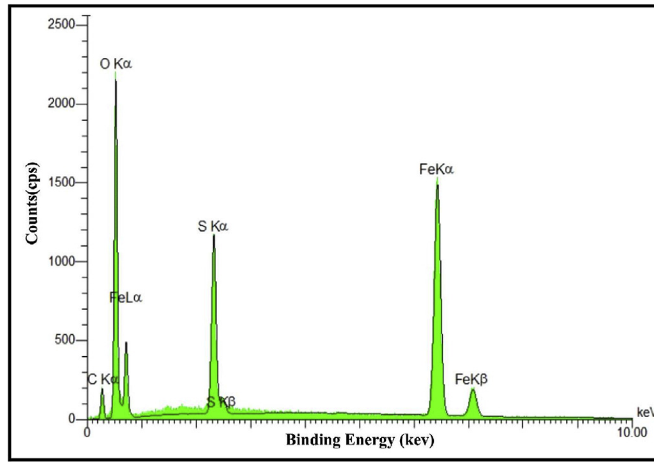

Fig. 2. The EDX analysis of the Fe_3O_4@PVA-SO_3H nanocomposite.

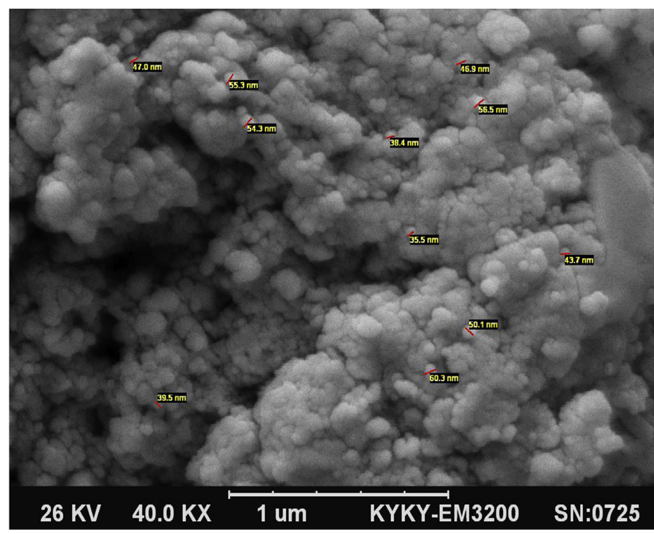

Fig. 3. The FE-SEM image of Fe_3O_4@PVA-SO_3H nanocomposite.

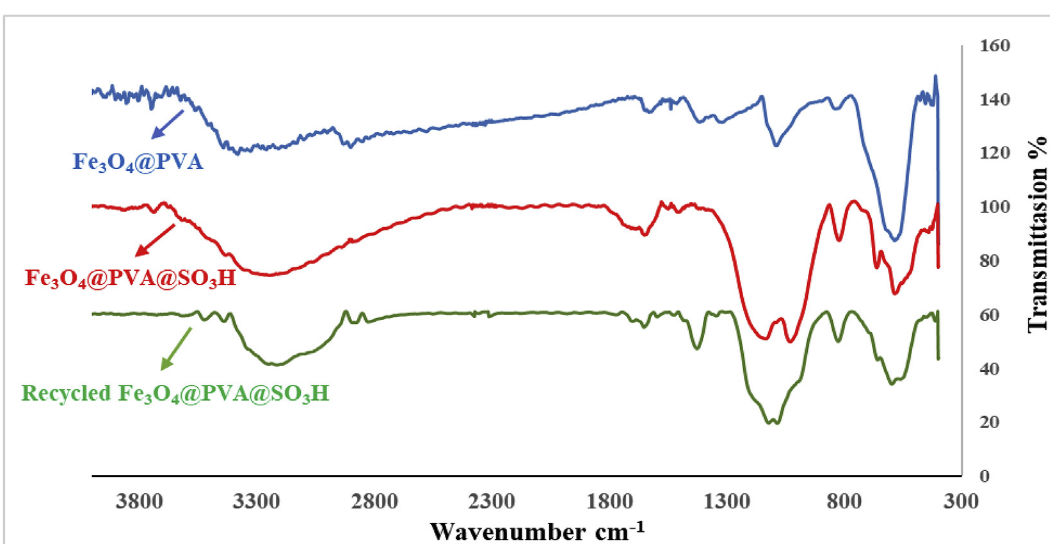

Fig. 1. The FT-IR spectra of Fe_3O_4@PVA, Fe_3O_4@PVA-SO_3H and the recycled Fe_3O_4@PVA-SO_3H.

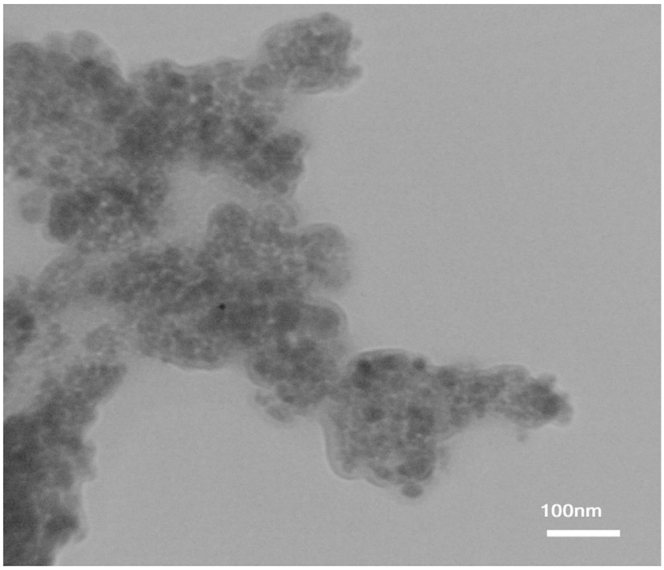

Fig. 4. The TEM image of Fe_3O_4@PVA-SO_3H nanocomposite.

monodisperse in gray colour. This analysis completely can confirm the successful synthesis of the nanocomposite.

3.2.1. Thermogravimetric analysis (TGA)

The thermogravimetric analysis (TGA) curve, display the relation between temperature and weight loss of the nanocatalysts (Fig. 5). Decomposition of the nanocomposite was achieved while heating at a rate of 10 °C/min in the air between 20 °C and 800 °C. As can be seen, the weight loss in the temperature range from 50 to 150 °C is related to the removal of the surface adsorbed water and weakly absorbed impurities. For the Fe_3O_4@PVA-SO_3H, the new weight loss about 40% in the temperature range of 200–550 °C assigned to the decomposition of PVA and SO_3H groups. Moreover, can be seen that the nanocomposite has a higher thermal stability compared to PVA alone that is decomposition at about 250 °C [39]. This result shows the strong interaction in the nanocomposite.

3.2.2. X-ray diffraction (XRD)

XRD measurement is used to determine crystalline nature of nanocomposite. Fig. 6 shows the X-ray diffraction patterns of Fe_3O_4@PVA-SO_3H and confirm the presence of Fe_3O_4 NPs on PVA. The broad diffraction peak around $2\theta = 20$ corresponds to PVA [40]. All of the observed peaks for the Fe_3O_4 are in perfect match with the characteristic data of magnetite iron oxide (JCPDS card No. 01-075-0449). The crystalline peaks of magnetite iron oxide with cubic structure observed at the diffraction angles (2θ) of 18.59, 30.53, 35.86, 37.53, 43.54, 54.13, 57.55, and 63.31. Peak broadening and peak high lowering of Fe_3O_4 are due to the grafting of nanoparticles on the surface of the PVA with amorphous nature. Furthermore, the particle size of Fe_3O_4/PVA-SO_3H nanocomposite was calculated by Debye–Scherrer equation. As a result, the average crystallite size was around 28 nm.

3.2.3. Vibrating sample magnetometer (VSM)

VSM analysis was applied at room temperature to measure magnetic properties (Fig. 7). The saturation magnetization values of Fe_3O_4@PVA and Fe_3O_4@PVA-SO_3H nanocomposite were around 32.95 and 24.15 emu g^{-1}. The decrease of the saturation magnetization of Fe_3O_4@PVA after loading to the SO_3H groups confirmed

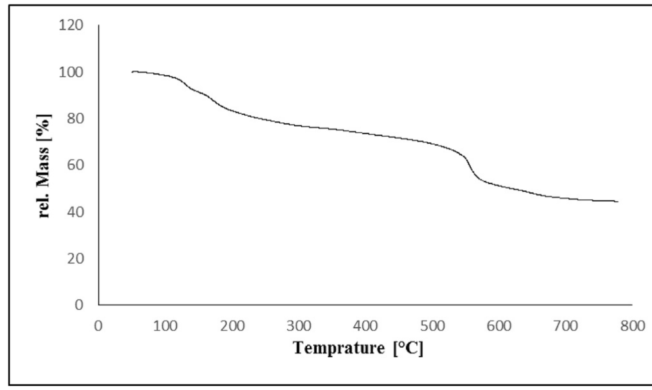

Fig. 5. The TGA curve of Fe_3O_4/PVA-SO_3H nanocomposite.

the successful synthesis of the nanocomposite. Moreover, the both of Fe_3O_4@PVA and Fe_3O_4@PVA-SO_3H show an acceptable magnetic property.

3.2.4. Back titration of Fe_3O_4@PVA-SO_3H in aqueous media

Acidity ($[H^+]$) of the synthesized Fe_3O_4@PVA-SO_3H nanocatalyst was achieved by the back titration method. At first, 0.5 g of Fe_3O_4@PVA-SO_3H, 0.5 g of NaCl, and 10 mL of NaOH 0.1 M were added to 35 mL of distilled water and stirred with a magnet for 24 h. After that, a few drops of phenolphthalein were supplemented into the mixture and the colour changed to pink. Finally, the mixture was titrated by the solution of HCl 0.1 M to reach the neutral pH. Accordingly, the pH of the nanocatalyst was calculated 1.61.

3.3. Application of the nanocatalyst in organic synthetic reaction

In this work, α-aminonitrile derivatives were synthesized by the reaction of different aromatic aldehydes with aniline and TMSCN in the presence of Fe_3O_4@PVA-SO_3H as a recoverable magnetic nanocatalyst in ethanol at room temperature. The work-up procedure of the product was easy as the nanocatalyst can be separated simply by an external magnet. To optimize the reaction conditions, a series of experiments were performed with the variation of different reaction parameters such as solvent and amount of catalyst for a representative condensation of 4-chlorobenzaldehyde (1 mmol), aniline (1 mmol) and TMSCN (1.2 mmol) as the model reaction. The results are summarized in Table 1. Fe_3O_4 NPs and Fe_3O_4@PVA are able to produce relatively low yields in EtOH, but, in the presence of Fe_3O_4@PVA-SO_3H nanocomposite, the yield of the product increased to 99% (Table 1, entry 5). The model reaction was also studied in various solvents such as H_2O, EtOH, EtOAc, and $CHCl_3$. The best result was achieved in EtOH. Also, different amount of the catalyst was investigated. As can be seen in Table 1, entry 5, in the presence of 50 mg of the catalyst, a significant yield was obtained. While the yield of the desired product **4b** was not significantly improved in presence of excess amount of the catalyst (Table 1, entries 11 and 12). The best result was obtained by carrying out the reaction at ambient conditions in ethanol for 10 min using 50 mg of Fe_3O_4@PVA-SO_3H.

In order to demonstrate the repeatability of this strategy, a broad variety of aromatic aldehydes possessing electron-withdrawing and electron-releasing substitutions, were employed and a variety of products were synthesized under the optimized conditions at room temperature. The desirable results of study are shown in Table 2. All the utilized aldehydes supplied the desired products in high yields and short reaction times.

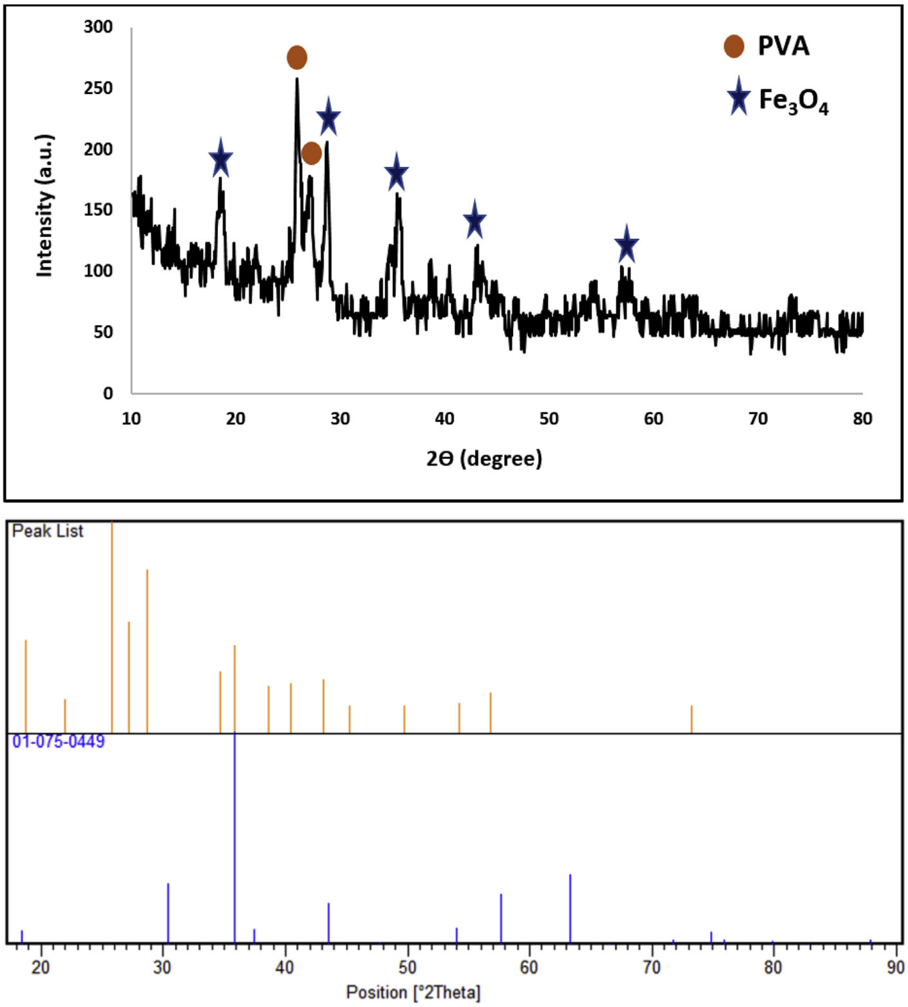

Fig. 6. The XRD pattern of: (a) Fe_3O_4@PVA-SO_3H nanocomposite, (b) the reference Fe_3O_4.

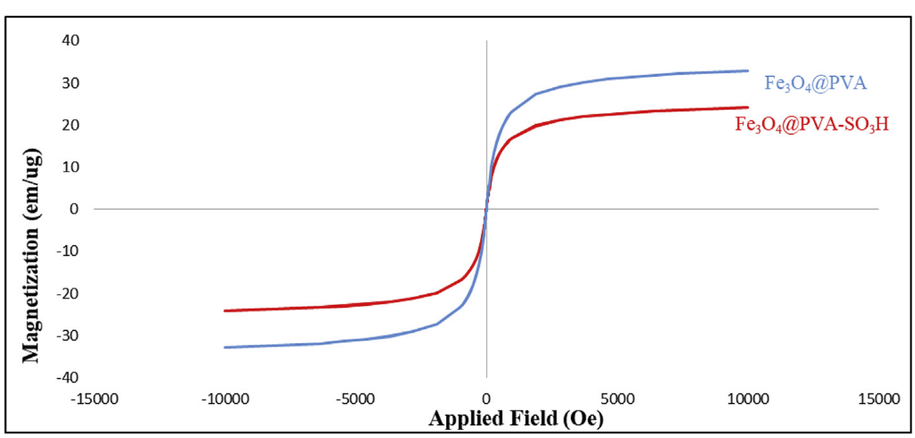

Fig. 7. The VSM curves of Fe_3O_4@PVA and Fe_3O_4@PVA-SO_3H nanocomposite.

3.4. Comparison the efficiency of synthesized nanocatalyst

To investigate the efficiency of Fe_3O_4@PVA-SO_3H catalyst with some other reported works for the synthesis of α-aminonitrile derivatives, the model reaction of benzaldehyde, aniline and TMSCN was compared with other previous reports. Most of last reports have disadvantages such as long time reaction, toxic solvent and low efficiency can be seen in Table 3, the results of the present work is more reliable than previous ones.

Table 1
Optimization of reaction conditions by reaction of 4-chlorobenzaldehyde, aniline and TMSCN at room temperature.

Entry	Solvent	Catalyst	Amount of catalyst (mg)	Temperature (°C)	Yield[a] (%)
1	EtOH	Fe_3O_4	50	r.t.	50
2	EtOH	PVA	50	r.t.	trace
3	EtOH	Fe_3O_4@ PVA	50	r.t.	35
4	H_2O	Fe_3O_4@PVA-SO_3H	50	r.t.	47
5	EtOH	Fe_3O_4@PVA-SO_3H	50	r.t.	96
6	EtOAc	Fe_3O_4@PVA-SO_3H	50	r.t.	55
7	$CHCl_3$	Fe_3O_4@PVA-SO_3H	50	r.t.	56
8	Solvent-free	Fe_3O_4@PVA-SO_3H	50	r.t.	45
9	EtOH	Fe_3O_4@PVA-SO_3H	20	r.t.	53
10	EtOH	Fe_3O_4@PVA-SO_3H	32	r.t.	60
11	EtOH	Fe_3O_4@PVA-SO_3H	70	r.t.	96
12	EtOH	Fe_3O_4@PVA-SO_3H	100	r.t.	96
13	EtOH	Fe_3O_4@PVA-SO_3H	50	60	35
14	EtOH	Fe_3O_4@PVA-SO_3H	50	Reflux	40

[a] Isolated yield.

Table 2
Synthesis of α-aminonitrile derivatives **4a-z** in optimal conditions.[a]

Entry	R^1	R^2	Product	Time (min)	Yield[b] (%)	Mp (°C)	
						Obs.	Lit.
1	Phenyl	H	**4a**	5	96	70–83	73-75 [41]
2	4-Chlorophenyl	H	**4b**	5	97	91–93	92-94 [42]
3	4-Bromophenyl	H	**4c**	5	98	102–104	100-101 [41]
4	3-Nitrophenyl	H	**4d**	5	90	88–90	89-90 [41]
5	4-Methoxylphenyl	H	**4e**	10	90	91–92	91-92 [41]
6	4-Nitrophenyl	H	**4f**	5	98	86–88	86-88 [41]
7	4-Hydroxyphenyl	H	**4g**	15	89	124–126	124-125 [41]
8	4-Methylphenyl	H	**4h**	15	91	71–73	70-71 [41]
9	4-Fluorophenyl	H	**4i**	5	96	101–102	99-101 [43]
10	2-Thienyl–	H	**4j**	10	85	97–99	97–99 [44]
11	2-Furanyl	H	**4k**	10	89	73–75	72–74 [44]
12	4-(Dimethylamino)phenyl	H	**4l**	15	90	107–109	107–110 [44]
13	4-Cyanophenyl	H	**4m**	5	98	112–114	113–115 [45]
14	3,4,5-Trimethoxyphenyl	H	**4n**	10	96	146–148	147–149 [43]
15	4-Hydroxy-3-methoxyphenyl	H	**4o**	20	88	114–116	113–115 [45]
16	2-Nitrophenyl	H	**4p**	15	89	135–137	135-137 [41]
17	2,6-Dichlorophenyl	H	**4q**	15	85	74–76	75–78 [44]
18	Cinnamaldehyde	H	**4r**	10	95	118–120	117-118 [46]
19	2-Chlorophenyl	H	**4s**	20	84	69–71	69-70 [45]
20	3-Fluorophenyl	H	**4t**	5	90	91–93	91-92 [47]
21	Phenyl	4-Me	**4u**	5	97	106–108	105–107 [45]
22	4-Chlorophenyl	4-Me	**4v**	5	97	87–89	85-87 [43]
23	Cinnamaldehyde	4-Me	**4w**	10	96	104–106	103-106 [45]
24	4-Methylphenyl	4-Me	**4x**	10	92	116–118	116-118 [45]
25	4-Nitrophenyl	4-Me	**4y**	5	97	84–86	83-85 [44]
26	Phenyl	4-NO_2	**4z**	30	68	128–129	128-129 [48]

[a] Reaction conditions: benzaldehyde (1 mmol), aniline (1 mmol) and TMSCN (1.2 mmol) and Fe_3O_4@PVA-SO_3H composite (0.05 g) at room temperature in 5 mL of ethanol.
[b] Isolated yield.

Table 3
Comparison the efficiency of the synthesized nanocatalyst with other reported works.

Entry	Catalyst	Condition	Time	Yield (%)	Ref
1	$InCl_3$	THF/r.t.	6 h	75	[49]
2	(Bromodimethyl)sulfonium bromide	CH_3CN/r.t.	1 h	89	[50]
3	$RuCl_3$ (20 mol %)	CH_3CN/r.t.	20 h	74	[51]
4	PVP-SO_2	CH_2Cl_2/50 °C	6 h	86	[52]
5	$Fe(ClO_4)_3$	CH_3CN/r.t.	3 h	95	[53]
6	Fe_3O_4@PVA-SO_3H	EtOH/r.t.	5min	98	This work

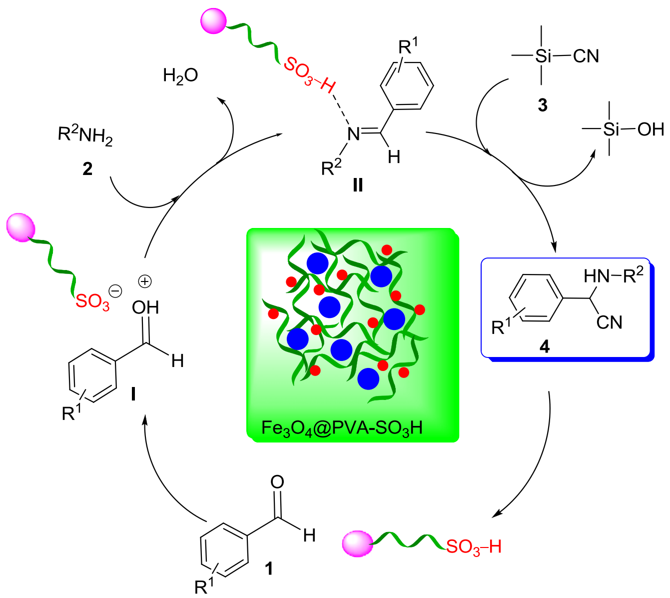

Scheme 2. Proposed mechanism for the synthesis of **4a-z** by using Fe_3O_4@PVA-SO_3H.

3.5. Mechanistic evaluation

A proposed mechanism for the formation of α-aminonitrile derivatives is shown in Scheme 2. In the first step, carbonyl of aldehyde was activated by Fe_3O_4@PVA-SO_3H catalyst, intermediate **I** was formed. Iminium intermediate **II** was formed by the condensation reaction between intermediate **I** and different amines **2** in the presence of the catalyst. according to the literature [44], the nucleophilic attack of TMSCN into imine yielded the products **4a-z**.

3.6. Catalyst recycling

A valuable property for a catalyst is its easy recovery and reusability. Therefore, in order to further evaluation of the nanocatalyst, after completion of the reaction, the catalyst was separated with an external magnet, washed with ethanol and water and dried after each run, and then reused in the next runs under the same ratio of catalyst and other reaction conditions to the model reaction. The results shows that the catalyst show no considerable reduction in activity within 10 cycles (Fig. 8). Also, recoverability and reusability of the catalyst without any decrease in catalytic activity after several times show catalyst stability.

4. Conclusions

In this research, Fe_3O_4@PVA-SO_3H with particular properties such as eco-friendly, high efficiency, green chemistry properties, non-expensive and easy separation was prepared in two steps. PVA with hydroxyl functional groups can be modified by MNPs and SO_3H groups. The nanocomposite was characterized by FT-IR, EDX, FE-SEM, XRD, TEM and TGA analyses. The FT-IR spectra demonstrated that SO_3H groups were successfully grafted onto the Fe_3O_4@PVA nanocomposite. The two major stages of degradation, corresponding to physical absorption and the organic phase of PVA and SO_3H were clearly displayed in TGA analysis. Also, XRD pattern and FE-SEM images supported the FT-IR and TGA results and confirmed the preparation of the nanocomposite. This efficient nanocomposite was also applied as a novel nanocatalyst for the synthesis of an important α-aminonitrile derivatives in high yields. The nanocatalyst was derived out by an external magnet and reused ten times with high efficiency. This is the first report on design, synthesis and characterization of the present nanocomposite and its application as an efficient catalyst with high reusability and stability.

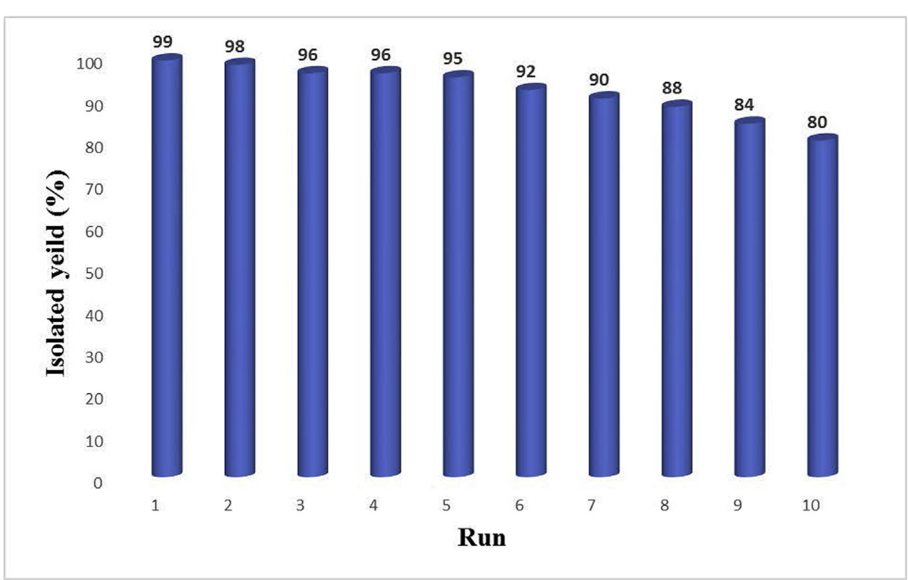

Fig. 8. Recycling diagram of Fe_3O_4@PVA-SO_3H nanocatalyst in the synthesis of **4b**.

Conflicts of interest

None of the authors have any competing or conflict of interests in the manuscript.

Acknowledgements

The authors gratefully acknowledge the partial support from the Research Council of the Iran University of Science and Technology.

References

[1] D. Ghanbari, M. Salavati-Niasari, J. Ind. Eng. Chem. 24 (2014) 284–292.
[2] A. Maleki, RSC Adv. 4 (2014) 64169–64173.
[3] A. Maleki, M. Azizi, Z. Emdadi, Green Chem. Lett. Rev. 11 (2018) 573–582.
[4] A. Maleki, Tetrahedron 68 (2012) 7827–7833.
[5] A. Maleki, Ultrason. Sonochem. 40 (2018) 460–464.
[6] A. Maleki, M. Ghassemi, R. Firouzi Haji, Pure Appl. Chem. 90 (2018) 387–394.
[7] A. Maleki, Tetrahedron Lett. 54 (2013) 2055–2059.
[8] A. Maleki, M. Aghaie, Ultrason. Sonochem. 39 (2017) 534–539.
[9] A. Maleki, H. Movahed, P. Ravaghi, Carbohydr. Polym. 156 (2017) 259–267.
[10] A. Maleki, P. Ravaghi, H. Movahed, Micro Nano Lett. 13 (2018) 591–594.
[11] A. Maleki, M. Aghaie, Ultrason. Sonochem. 39 (2017) 534–539.
[12] A. Maleki, R. Firouzi-Haji, Sci. Rep. 8 (2018), https://doi.org/10.1038/s41598-018-35676-x, 17303.
[13] A. Maleki, Helv. Chim. Acta 97 (2014) 587–593.
[14] A. Maleki, M. Aghaei, N. Ghamari, M. Kamalzare, Int. J. Nanosci. Nanotechnol. 12 (2016) 215–222.
[15] A. Maleki, R. Ghalavand, R. Firouzi-Haji, Iran. J. Catal. 8 (2018) 221–229.
[16] A. Maleki, J. Rahimi, J. Porous Mater. 25 (2018) 1789–1796.
[17] A. Maleki, R. Firozi-Haji, Z. Hajizadeh, Int. J. Biol. Macromol. 116 (2018) 320–326.
[18] M. Zhang, Y.H. Liu, Z.R. Shang, H.C. Hu, Z.H. Zhang, Catal. Commun. 88 (2017) 39–44.
[19] A. Maleki, J. Rahimi, O.M. Demchuk, A.Z. Wilczewska, R. Jasiński, Ultrason. Sonochem. 43 (2018) 262–271.
[20] S. Mallakpour, F. Derakhshan, High Perform. Polym. 27 (2015) 458–468.
[21] S. Xu, W. Yu, X. Yao, Q. Zhang, Q. Fu, Compos. Sci. Technol. 131 (2016) 67–76.
[22] X. Lu, M. Niu, R. Qiao, M. Gao, J. Phys. Chem. B 112 (2008) 14390–14394.
[23] D. Ghanbari, M. Salavati-Niasari, M. Ghasemi-Kooch, Particuology 26 (2016) 87–94.
[24] D. Ghanbari, M. Salavati-Niasari, M. Ghasemi-Kooch, J. Ind. Eng. Chem. 20 (2014) 3970–3974.
[25] S. Kayal, R.V. Ramanujan, Mater. Sci. Eng. C 30 (2010) 484–490.
[26] Y. Wei, X. Zhang, Y. Song, B. Han, X. Hu, X. Wang, Y. Lin, X. Deng, Biomed. Mater. 6 (2011), 055008.
[27] H. Jia, F. Huang, Z. Gao, C. Zhong, H. Zhou, M. Jiang, P. Wei, Biotechnol. Rep. 10 (2016) 49–55.
[28] P. Mendoza Zélis, D. Muraca, J.S. Gonzalez, G.A. Pasquevich, V.A. Alvarez, K.R. Pirota, F.H. Sanchez, J. Nano Res. 15 (2013) 1613–1616.
[29] A. Maleki, Z. Hajizadeh, R. Firouzi-Haji, Microporous Mesoporous Mater. 259 (2018) 46–53.
[30] M. Zhang, P. Liu, Y.H. Liu, Z.R. Shang, H.C. Hu, Z.H. Zhang, RSC Adv. 6 (2016) 106160–106170.
[31] A. Shaabani, A. Maleki, Appl. Catal. A, Gen. 331 (2007) 149–151.
[32] J.S. Yadav, A. Antony, J. George, B.V. Subba Reddy, Curr. Org. Chem. 14 (2010) 414–424.
[33] S.K. De, R.A. Gibbs, Tetrahedron Lett. 45 (2004) 7407–7408.
[34] S.K. De, Beilstein J. Org. Chem. 1 (2005) 8.
[35] A. Maleki, Z. Hajizadeh, H. Abbasi, Carbon Lett. 27 (2018) 42–49.
[36] M.N. Chen, L.P. Mo, Z.S. Cui, Z.H. Zhang, Curr. Opin. Green Sustain. Chem. 15 (2019) 27–37.
[37] S.-Y. Kim, B. Ramaraj, K.R. Yoon, Surf. Interface Anal. 44 (2012) 1238–1242.
[38] Z. Hajizadeh, A. Maleki, Mol. Catal. 460 (2018) 87–93.
[39] T. Abdul Kareem, A. Anu kaliani, Arab. J. Chem. 4 (2011) 325–331.
[40] H.Z. Li, S.C. Chen, Y.Z. Wang, Compos. Sci. Technol. 115 (2015) 60–65.
[41] A. Maleki, R. Firozi-Haji, M. Ghassemi, H. Ghafuri, J. Chem. Sci. 129 (2017) 457–462.
[42] A. Maleki, H. Movahed, R. Paydar, RSC Adv. 6 (2016) 13657–13665.
[43] K. Niknam, D. Saberi, M.N., Tetrahedron Lett. 51 (2010) 2959–2962.
[44] H. Ghafuri, A. Rashidizadeh, B. Ghorbani, M. Talebi, New J. Chem. 39 (2015) 4821–4829.
[45] M. Eslami, M.G. Dekamin, L. Motlagh, A. Maleki, Green Chem. Lett. Rev. 11 (2018) 36–46.
[46] A. Shaabani, A. Maleki, M.R. Soudi, H. Mofakham, Catal. Commun. 10 (2009) 945–949.
[47] A. Mobaraki, B. Movassagh, B. Karimi, ACS Comb. Sci. 16 (2014) 352–358.
[48] X.L. Zhang, Q.P. Wu, Q.S. Zhang, J. Chem. Res. 37 (2013) 690–693.
[49] B.C. Ranu, S.S. Dey, A. Hajra, Tetrahedron 58 (2002) 2529–2532.
[50] B. Das, R. Ramu, B. Ravikanth, K.R. Reddy, Synthesis 9 (2006) 1419–1422.
[51] S.K. De, Synth. Commun. 35 (2005) 653–655.
[52] G.A. Olah, T. Mathew, C. Panja, K. Smith, G.K. Surya Prakash, Catal. Lett. 114 (2007) 1–7.
[53] H.A. Oskooie, M.M. Heravi, A. Sadnia, F. Jannati, F.K. Behbahani, Synth. Commun. 37 (2007) 2543–2548.